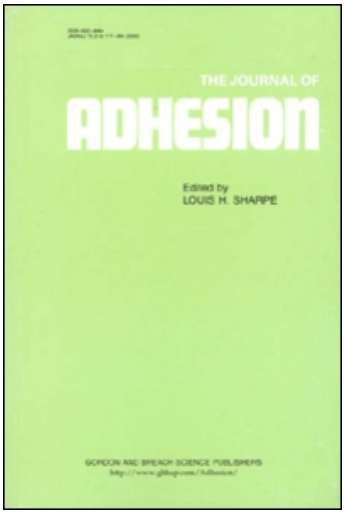

The Journal of Adhesion
Publication details, including instructions for authors and subscription information:
http://www.informaworld.com/smpp/title~content=t713453635

Comparison of Peel Tests for Metal-Polymer Laminates for Aerospace Applications

L. F. Kawashita[a]; D. R. Moore[a]; J. G. Williams[a]
[a] Mechanical Engineering Department, Imperial College London, London, UK

To cite this Article Kawashita, L. F. , Moore, D. R. and Williams, J. G.(2005) 'Comparison of Peel Tests for Metal-Polymer Laminates for Aerospace Applications', The Journal of Adhesion, 81: 6, 561 — 586
To link to this Article: DOI: 10.1080/00218460590954557
URL: http://dx.doi.org/10.1080/00218460590954557

The Journal of Adhesion, 81:561–586, 2005

ISSN: 0021-8464 print/1545-5823 online
DOI: 10.1080/00218460590954557

Taylor & Francis
Taylor & Francis Group

Comparison of Peel Tests for Metal–Polymer Laminates for Aerospace Applications

L. F. Kawashita
D. R. Moore
J. G. Williams
Mechanical Engineering Department, Imperial College London, London, UK

Standard peel tests for aerospace laminates based on metal–polymer systems, namely floating-roller and climbing-drum peel methods, have been accommodated in a unified theory of peeling. This theory also accommodates more basic peel tests such as T-peel and fixed-arm peel and also newer methods such as mandrel peel. These five methods have been applied to two aerospace laminate systems to critically examine their use in the determination of adhesive strength. The theory has been used to unify the outputs from the tests in terms of adhesive fracture toughness. In this way, the comparative merits of the methods can be commented on.

The validity of the standard methods has been put in doubt because of the absence of a correction for plastic bending energy and also because of the poor conformance of the peel arm to the roller system used in these methods. The unified theory and some measurements of peel-arm curvature help but not completely overcome some of these difficulties.

A further complication that arises in peel is a change in the plane of fracture. This reflects a transition from cohesive fracture in the adhesive to an adhesive fracture at the interfaces among adhesive, primer, and substrate. It is likely that such plane-of-fracture phenomena are intrinsic to evaluation of the laminate and that contemplation of cohesive fracture toughness for the adhesive cannot accommodate such events.

Keywords: Fracture toughness; Peeling; Structural adhesives; Adhesive joints; Climbing drum; Floating roller; Fixed arm peel; T-peel; Mandrel peel; Plastic bending corrections; Cohesive fracture toughness; Peel strength

Received 19 July 2004; in final form 15 February 2005.
Address correspondence to D. R. Moore, Mechanical Engineering Department, Imperial College London, Room 806, South Kensington Campus, Exhibition Road, London SW7 2AZ, UK. E-mail: r.moore@imperial.ac.uk

INTRODUCTION

Laminates made of aluminium alloys and epoxy adhesives are commonly used in aerospace applications. The strength of the bond is a critical issue because the laminates act as engineering structures. Consequently, the strength of the bond is measured as a requirement for the application. This measurement is made by the determination of peel strength, that is, the force per unit width required to peel the structure apart. A number of standard methods have been established for conducting this test, with a climbing-drum peel [1] and a floating-roller peel [2] being two such approaches.

In a general sense, a measurement of peel strength does not separate the contributions from adhesive fracture energy and plastic bending energy. Instead, it equates adhesive strength with the total energy required to peel the structure apart. A number of workers have reported analytical approaches where the plastic bending energy can be calculated [3–5]. Their analyses have been applied to the peeling of polymer–metal laminate systems, and it is not unusual to find plastic energy contributions of up to 90% of the input energy applied to the laminate [6]. This suggests that the use of peel strength alone might be worthy of review.

These analytical approaches have been used with peel methods such as fixed-arm peel and T-peel [6]. In fact, these peel tests have also been standardised in their own right in terms of measuring adhesive strength through a measurement of peel strength [7, 8]. However, when the analytical calculations are combined with the peel-strength measurement, then a value of adhesive fracture toughness can be obtained (G_A).

The analytical approaches will correct a possibly large error in the determination of adhesive fracture toughness, particularly when there is a high plastic bending contribution. Nevertheless, the accuracy of the calculations depends on the precision in the analysis and the accuracy of the experimental parameters required for the calculations. The latter are in two forms, first, a peel-strength measurement for either a fixed-arm or T-peel procedure. Second, a description of the tensile stress-strain behaviour of the peel arm(s) that needs to be modelled either as a bilinear function or as a linear-power law function to make the calculations tractable [5]. Inevitably, there will be errors associated with such calculations and, therefore, it would be helpful to review these methods.

The mandrel peel test [9] does not rely on any of these approaches but instead provides a direct experimental route for the determination of adhesive fracture toughness [9, 10]. Such an approach involves the conformation of the peel arm to a roller by the application of an

alignment force. In the mandrel test, a global energy analysis can be used to determine both adhesive fracture toughness and plastic bending energy by direct experimentation. Consequently, it would be helpful to compare this method with outputs from the other methods already mentioned.

The aim of this work is to apply all five methods to the measurement of peel strength and adhesive fracture toughness for two experimental aerospace laminates. This requires the following steps:

(1) A global-energy analysis of the climbing-drum peel and the floating-roller peel methods to derive expressions for adhesive fracture toughness from the usual peel-strength measurement.
(2) A critical review of the calculations involved in the fixed-arm peel and T-peel procedures, and the development of an experimental method for the determination of the radius of curvature of the peel arm, because this is a key parameter involved in the analytical methods.
(3) Application of the mandrel peel test with the aim of providing an alleged credible value of the adhesive fracture toughness that can act as a reference.

Finally, it is intended to provide critical and constructive comment from this work in terms of using peel methods to assess and select adhesives for aerospace applications.

ANALYTICAL APPROACHES

All the tests discussed here are variants on the roller modified peel test. The basic form of the peel test is shown in Figure 1 in which a flexible strip of thickness, h, and width, b, is peeled from a substrate by pulling the strip with a force, F, at an angle θ. The total energy per unit area, G, dissipated in debonding the strip is given in Equation 1 [3], which assumes an infinitely stiff peel arm and neglects residual stresses:

$$G = \frac{F}{b}(1 - \cos\theta). \tag{1}$$

Unless the strip is entirely elastic, some of this energy goes into plastic bending, G_P, creating a local radius of curvature, R_0, at the load point and subsequent straightening or unbending [5]. The true adhesive toughness, G_A, is thus

$$G_A = G - G_P(R_0) \tag{2}$$

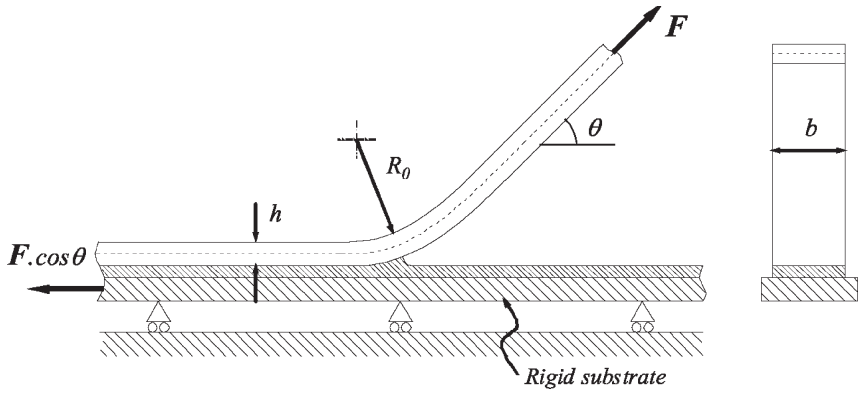

FIGURE 1 Basic peel test.

and G_P can be calculated from the properties of the strip and conditions at the bonding point.

An alternative approach is to control the curvature by forcing the strip to conform to a roller by applying a horizontal force, D, as shown in Figure 2. At the debonding point, we have an angle, θ, and a force, F, as shown, but the applied force, P, is at an angle θ_1 to the vertical. For low friction, equating the moments around the axis, we have

$$FR_1 = PR_1, \quad \text{i.e.,} \; F = P \tag{3}$$

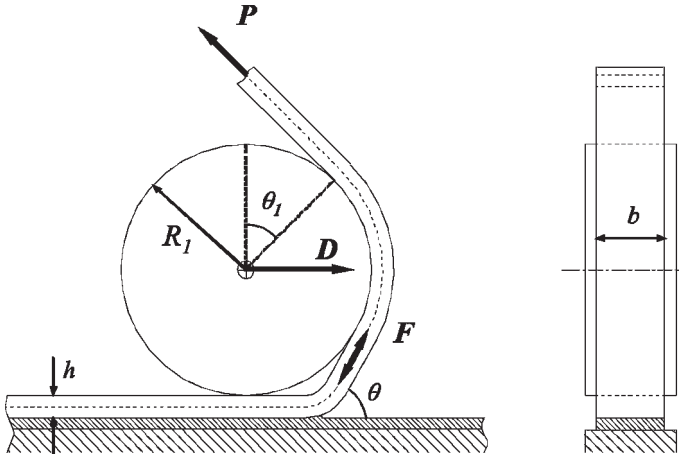

FIGURE 2 Roller-assisted peeling.

and horizontal equilibrium gives an expression for the force D,

$$D = P(\cos\theta + \cos\theta_1). \tag{4}$$

Thus,

$$\cos\theta = \frac{D}{P} - \cos\theta_1$$

and

$$G = \frac{F}{b}(1 - \cos\theta) = \frac{P}{b}(1 + \cos\theta_1) - \frac{D}{b}. \tag{5}$$

Two ASTM standards [1,2] use variants of this system. Figure 3 shows the floating-roller test where the geometry makes $\theta_1 = 63.7^\circ$ and $D/P = \cos\theta_1 = 0.44$. Thus, $\cos\theta = 0$, that is, $\theta = 90^\circ$ and $G = P/b$. If R_0 at debonding is less than R_1 (12.7 mm), then the strip will bend to R_0 and unbend to R_1 so that for $R_0 > R_1$ there would be conformity to the roller. R_0 depends on h, θ, and G_A, and so it is not possible to know if there will be conformity *a priori*.

If there is conformity, then G_P is determined by R_1, and this could be determined by performing a separate test on an unbonded strip and

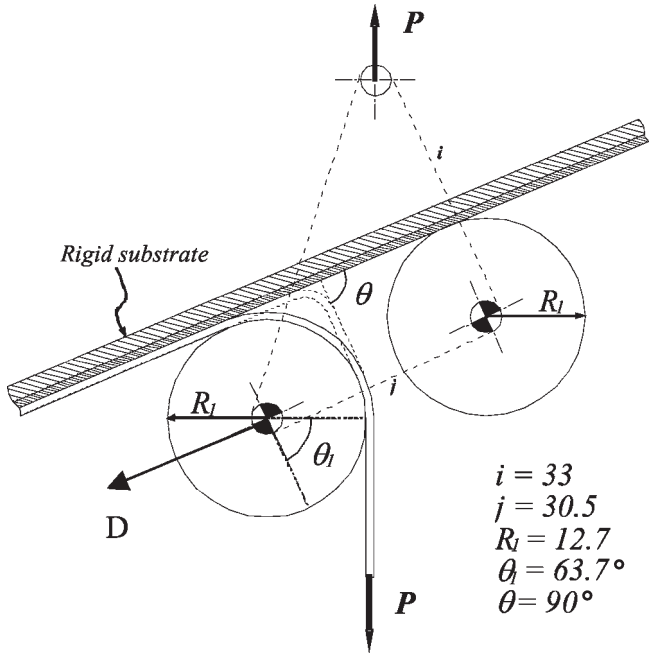

FIGURE 3 Floating-roller test.

measuring a force, P_0, and hence

$$G_A = \left(\frac{P - P_0}{b}\right). \tag{6}$$

Another popular variant is the climbing-drum test shown in Figure 4. Here $\theta_1 = 180^o$ that is, $\cos\theta_1 = -1$ and the loading must be applied *via* a radius $R_2 > R_1$. Thus,

$$\begin{aligned} F\cos\theta = P, \text{ also } \quad FR_1 = PR_2, \\ G = \frac{F}{b}(1 - \cos\theta) = \left(\frac{F - P}{b}\right) = \frac{P}{b}\left(\frac{R_2}{R_1} - 1\right), \end{aligned} \tag{7}$$

and

$$\cos\theta = \frac{R_1}{R_2}. \tag{8}$$

The same issues with regard to conformity arise as in the floating roller test and, if conformity occurs, an unbonded test may be performed to give P_0 and here

$$G_A = \left(\frac{P - P_0}{b}\right)\left(\frac{R_2}{R_1} - 1\right) \tag{9}$$

The mandrel test, described here, is a more versatile version in that D is applied independently and so θ changes; hence, R_0 changes and conformity can be achieved. In the tests described here, $\theta_1 = 90^\circ$,

$$\cos\theta = \frac{D}{P}, \tag{10}$$

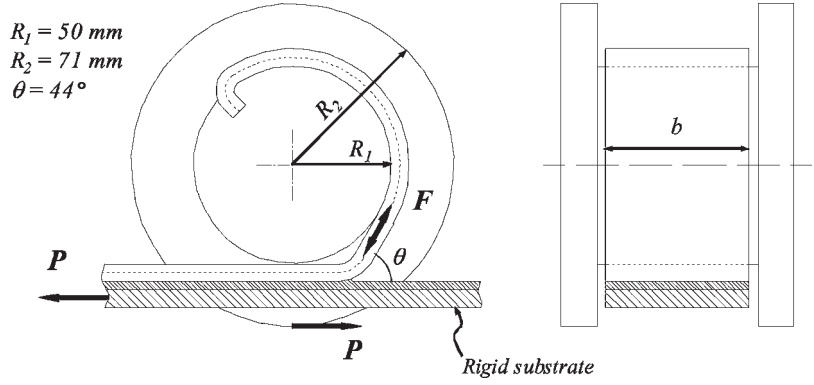

FIGURE 4 Climbing-drum test.

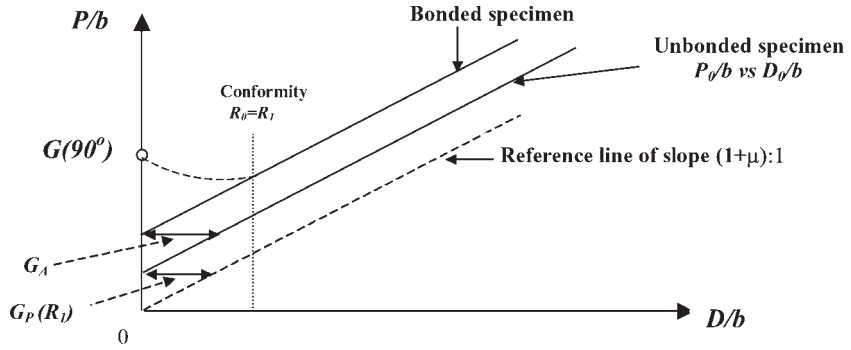

FIGURE 5 Data analysis for the mandrel test.

and

$$G = \left(\frac{P - D}{b}\right). \tag{11}$$

For an unbonded specimen, R_0 is large, conformity is guaranteed, and data in the form of P_0/b *versus* D/b is shown in Figure 5 with a slope of unity (for zero friction) but displaced by $G_P(R_1)$ as shown.

For the bonded specimen at $D = 0$, $\theta = 90^\circ$ so the value is as in the 90° peel test, and usually $R_0 < R_1$ and $P/b > G_P(R_0) + G_A > G_P(R_1) + G_A$. As D increases, θ decreases and R_0 increases until $R_0 = R_1$ and conformity occurs as shown. For larger D values, the lines should be parallel and displaced by G_A.

Generally the friction is low in such tests (coefficient of friction $\mu < 2\%$) but it is calibrated out, because to include friction, we have

$$P = F(1 + \mu)$$

and hence

$$\frac{P}{b} = \frac{D(1 + \mu)}{b} - G \tag{12}$$

so that the slope is $(1 + \mu)$ and the horizontal translation of the lines gives the G values.

Materials

Two aerospace epoxy–aluminium alloy laminates have been used in this work. Both laminates were bonded as 230 mm × 350 mm sheets with an unbonded portion (about 55 mm) in the long side. The sheet

was a sandwich of 2024-T3 aluminium alloy (AA) with a toughened epoxy compound at the centre. The top and bottom plates were 0.63 mm and 1.63 mm thick, respectively. Both AA substrates were treated in a FPL etching process potassium dichromate/sulfuric acid bath, (Forest Products Laboratory, Madison, WI, USA) and sprayed with an epoxy-based primer compound.

Two toughened epoxy adhesives were used, designated system A and system F. They were experimental compounds but both were candidates for aerospace applications. The primed AA plates were cured for 120 min at 133°C in an autoclave under pressure.

Various parallel strips were cut and subsequently machined, depending on the peel test configuration. Fixed-arm and mandrel peel specimens were of dimensions 15 mm × 305 mm, with bond lines 15 mm × 250 mm. Climbing-drum and floating-roller specimens were cut to the final dimensions suggested in the standard procedures [1, 2]. In all cases, the thick substrate acted as the base plate and was attached to the table on the peel jigs. Therefore, the 0.63-mm substrate always acted as a peel arm, and for the T-peel procedure both substrates were considered as peel arms.

Experimental Procedures

Climbing-drum and floating-roller peel tests were conducted on Instron (High Wycombe, UK) universal testing machines according to the procedures described in American Society for Testing and Materials (ASTM) standards [1, 2].

The floating roller peel apparatus is shown in Figure 6. Its construction differs from a standard jig in that a window was cut into the front plate to observe the peel arm around the floating roller during testing and to make measurements of the peel angles.

Figure 7 shows the arrangement for the climbing-drum procedure that follows the requirements of the test standard [2].

Fixed-arm peel and T-peel experiments were also conducted on Instron universal testing machines according to the test protocols described by the European Structural Integrity Society (ESIS) technical committee 4 [11]. Figure 8 shows the experimental arrangement for fixed-arm peel, where peel angles in the range 45° to 135° could be used. The base of the laminate was attached to a table located on a linear bearing system so that frictional forces were minimised during the peeling process.

T-peel experiments were conducted on an Instron testing machine by clamping each peel arm in the machine grips. However, it was

FIGURE 6 Floating-roller peel apparatus (see also Figure 3).

important to ensure that the peel arms did not touch the clamping equipment on the test machine during the peeling process. This possibility was enhanced by the stiffness difference in the two peel

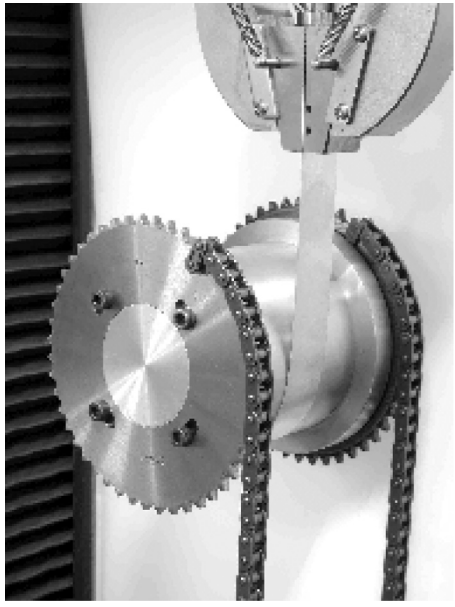

FIGURE 7 Climbing-drum peel apparatus (see also Figure 4).

FIGURE 8 Variable-angle fixed-arm peel apparatus.

arms resulting from their thickness difference (0.63 mm compared with 1.63 mm). The peel angle during the test was approximately 180°.

The mandrel peel equipment is shown in Figure 9 whilst others details are given in Reference 9. The base of the laminate is attached to a table that is positioned on a linear bearing system that minimises friction during the peeling process. The peel arm is bent around a circular roller (the mandrel) whilst an alignment force is applied to the base of the laminate. The roller incorporates ball bearings to further

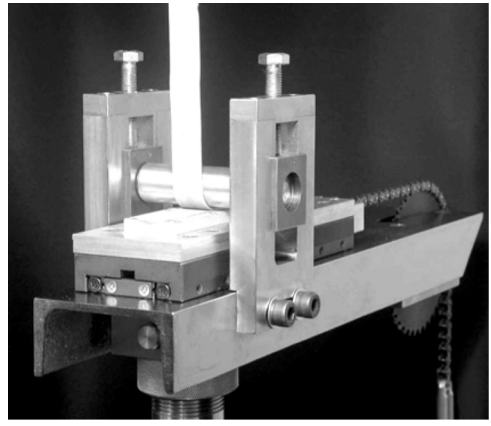

FIGURE 9 Mandrel peel apparatus (see also Figure 2).

reduce frictional effects. Mandrel radii were available in the range 5 mm to 20 mm, although for the particular laminates used in this work, only the 5-mm radius provided conformance of the peel arm to the mandrel. The peeling strip was attached to an Instron testing machine and peel force (P) was monitored as a function of alignment force (D).

Tensile stress-strain measurements were conducted on the peel-arm material to provide a necessary input to the calculations of adhesive fracture toughness. Parallel strip specimens were tested at 1 mm/min (strain rate of 2×10^{-3}) where an optical extensometer was used to measure axial strain.

RESULTS AND DISCUSSION

Tensile Stress-Strain of the Peel Arm

The adhesive fracture toughness is calculated from a combination of experimental measurements, namely peel strength and the tensile stress-strain behaviour of the peel arm material. The stress-strain curves are used to obtain elastic and plastic parameters based on bilinear or linear/power-law functions. These parameters allow the calculation of plastic bending energy [5] and software for this computation is available online [12]. The bilinear function fitted the data well, as shown in Figure 10. Table 1 summarises the parameters obtained from this fit that are used in the calculations of plastic bending energy.

Floating-Roller Peel

Floating-roller peel experiments on laminates with adhesives A and F showed that the peel arms did not conform to the roller, as shown in Figure 11.

The photographs in Figure 11 were taken when a steady-state peeling had been established. It can be seen that the extent of nonconformance to the roller is different, although did appear to be similar at the start of the peel process. Force *versus* displacement plots are shown in Figure 12. It is observed that the laminate with adhesive F exhibits a steady peel force throughout the process, whilst the laminate with adhesive A exhibits a fall in peel force until a steady value is obtained at the end. Observation of the laminates during peel showed that the laminate with adhesive A exhibited cohesive fracture at the start of the test. However, as the peel process continued, the plane

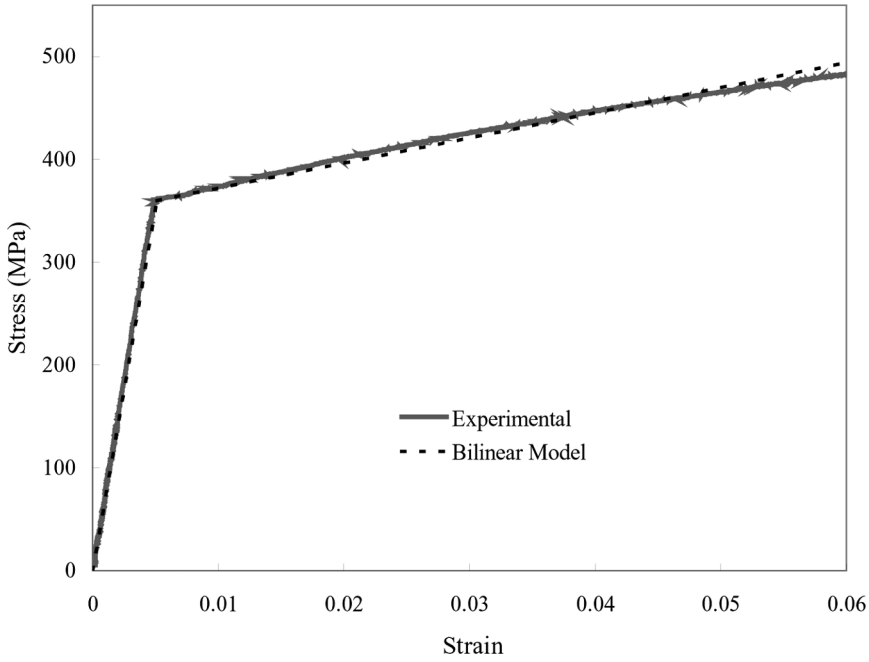

FIGURE 10 Experimental tensile stress-strain data with a bilinear function superimposed.

of fracture moved gradually to the interface between the adhesive and the substrate. The final locus of failure could be seen to be at the primer. The laminate with adhesive F exhibited cohesive fracture throughout the process and the peel force remained reasonably steady.

The observation of nonconformance of the peel arm to the roller is compatible with the theoretical analysis for the case that $R_1 > R_0$. (A debonded specimen test was, therefore, not required). Nevertheless, this nonconformance invalidates a conventional transfer from peel

TABLE 1 Tensile Properties of AA 2024-T3 Based on a Bilinear Fit to Experimental Data

Elastic modulus (E_1) (GPa)	Plastic modulus (E_2) (GPa)	Work hardening coefficient (α) (E_2/E_1)	Yield strain (%)	Yield stress (MPa)
70	2.5	0.035	0.51	360

FIGURE 11 Photographs of the floating-roller peel tests for the two laminate systems: a) adhesive A and b) adhesive F.

strength to adhesive fracture toughness, based on the peel-arm curvature being controlled by the roller radius.

The peel arm in the floating-roller test is sufficiently visible to enable high-resolution photography to be conducted and from these photographs, the actual radius of the peel arm can be determined. A digital camera with macro lenses produced clear photographs of the edge of the specimens during the tests. The digital images were then converted into two-dimensional coordinates from which the numerical curvatures could be calculated. This measured value of radius of curvature then enables the calculation of plastic work in bending and, consequently, the adhesive fracture toughness can be calculated. Table 2 summarises these results.

The actual radius of curvature of the peel arm is considerably smaller than the radius of the floating roller. Therefore, the condition described in Figure 3 with its accompanying analysis ($R_1 > R_0$) is

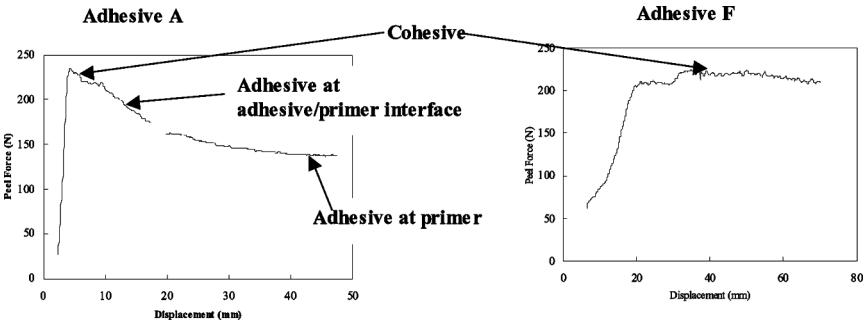

FIGURE 12 Peel force *versus* displacement for the floating roller test.

TABLE 2 Floating Roller Results Based on Measured Radius of Curvature for the Peel Arm

	G_A (J/m^2)	G (J/m^2)	G_P (J/m^2)	Measured R_0 (mm)	Plastic correction (%)
Adhesive F (cohesive fracture)	2000	10,510	8510	6.86	81
Adhesive A (adhesive fracture)	1270	6690	5420	9.31	80

Note: The radius of curvature of the floating roller is 12.7 mm.

confirmed. This difference in radii (between R_0 and R_1) indicates the error involved in conducting calculations based on an assumption of conformation. The peel-arm curvature is also different between the adhesives and, therefore, the laminate system will influence the degree of error associated in a standard analysis of peel strength from this procedure.

Climbing-Drum Peel

The climbing-drum procedure was conducted on both laminate systems and, in both cases, there was poor conformance of the peel arm to the circular drum. This is illustrated for adhesive F in Figure 13.

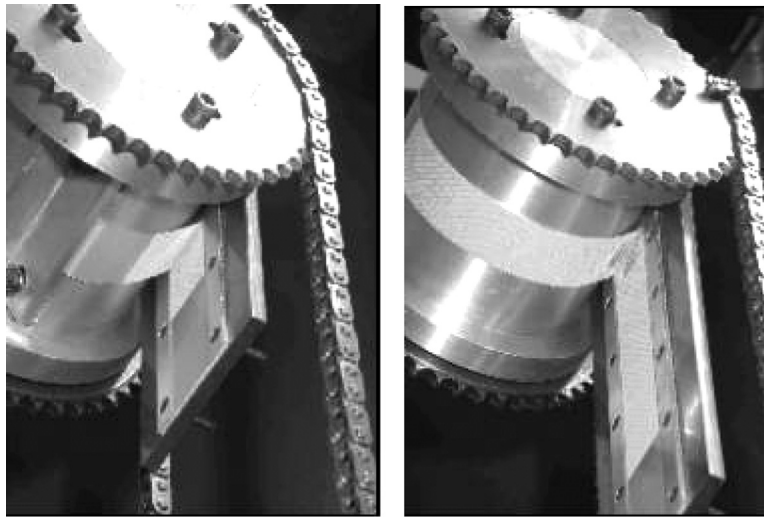

FIGURE 13 Climbing-drum test for adhesive F at the start and during the peeling process, illustrating poor conformance of the peel arm to the drum.

The geometric arrangement in the climbing-drum test did not accommodate photography of the peel arm in a way that would enable the radius of curvature to be measured. Neither was it possible to measure the angle θ as shown in Figure 4. Therefore, the test is invalid because of this nonconformance and application of a plastic bending correction to the data could not be undertaken. Consequently, the values of G_A that are calculated from this method, $7890\,J/m^2$ for adhesive F and $5460\,J/m^2$ for adhesive A, are hopelessly too large.

Fixed Arm and T-Peel

Variable-angle fixed-arm peel was conducted at three peel angles, namely 45°, 90°, and 135°. These experiments provided peel-strength data according to the test protocol documented in Reference 11. Peel strength could be converted to external input energy (G) and plastic bending energy (G_P) could be derived from the *ICPeel* software [12] by combining the peel data with tensile stress-strain data for the peel-arm material. Adhesive fracture toughness is then obtained by subtracting the plastic energy from the external input energy as indicated by Equation 2 [5]. For the laminate based on adhesive *F*, observation of the plane of fracture showed different peel mechanisms for the different peel angles. At a peel angle of 45°, the failure was cohesive in the adhesive. At a peel angle of 90°, there was some adhesive failure (*i.e.*, fracture at the adhesive-substrate interface), but mostly cohesive failure (*i.e.*, fracture only in the adhesive). At a peel angle of 135°, there was a larger contribution from adhesive failure. Peel force decreased as peel angle increased, but the magnitude of G increased. Therefore, it would seem that G influences the plane of fracture. Further details on the plane of fracture are discussed in a later section.

For the laminate based on adhesive A, observation of the locus of failure showed mainly adhesive fractures, with hints of cohesive failure. Again, the smaller the peel angle, the higher the contribution from cohesive failure, but at all peel angles, adhesive failure was dominant.

The T-peel tests on these laminates were dominated by the stiffness difference between the peel arms. One arm was much thicker than the other (1.63-mm AA compared with 0.63-mm AA). This thickness difference translated to a peel angle of almost 180°. Nevertheless, an analysis was conducted for each peel arm [11], and an overall adhesive fracture toughness value was determined.

The plane of fracture for both adhesive systems (F and A) in T-peel was a combination of cohesive and adhesive failure. For adhesive

TABLE 3 Summary of Fixed-Arm and T-Peel Results as Mean Values

Adhesive	Test method	G (J/m^2)	G_P (J/m^2)	$G_A = G - G_P$ (J/m^2)
Adhesive F	Fixed-arm 45°	9452	6353	3099
	Fixed-arm 90°	13080	10083	2997
	Fixed-arm 135°	13910	11660	2250
	T-peel	14700	13000	1700
Adhesive A	Fixed-arm 45°	5083	3504	1579
	Fixed-arm 90°	6069	4764	1305
	Fixed-arm 135°	6217	5189	1028
	T-peel	10133	8917	1216

F, the extent of adhesive failure was more than that experienced in the large-angle fixed-arm test. For adhesive A the extent of adhesive fracture was similar to that observed in the 90°-fixed-arm peel test.

The results from fixed-arm peel and T-peel are summarised in Table 3 in the form of mean values. Individual results are used in subsequent analysis.

The extent to which the external energy is corrected for plastic bending energy is an inherent source of error in the determination of adhesive fracture toughness. The plastic correction can be given by [11]

$$\text{correction } (\%) = \left(\frac{G_P}{G}\right) \times 100.$$

The greater the correction, the less certainty associated with the value of adhesive fracture toughness. Table 4 shows the corrections for both fixed-arm peel and T-peel test data, where it can be seen that the corrections for high peel angle and for T-peel are relatively large. Evidence has shown [6] that corrections around the 70% level can provide adequately accurate values of adhesive fracture toughness. Plastic corrections of 88% lie in uncharted waters.

The fixed-arm and the T-peel results for adhesive F are plotted in Figure 14. The graph includes external energy, plastic bending

TABLE 4 Plastic Corrections for Fixed-Arm and T-Peel Tests

Adhesive	Fixed-arm 45°	Fixed-arm 90°	Fixed-arm 135°	T-peel
Adhesive F	66%	76%	83%	88%
Adhesive A	67%	77%	83%	88%

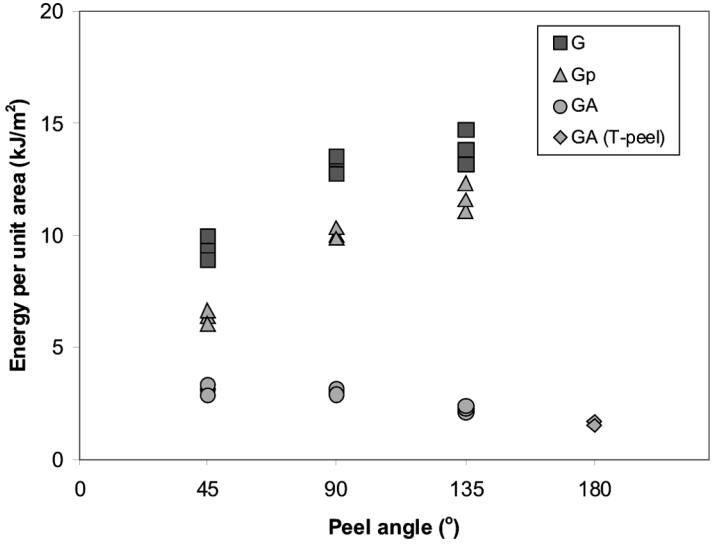

FIGURE 14 Fixed-arm and T-peel results for adhesive F.

energy, and adhesive fracture toughness for the fixed arm tests, but only adhesive fracture toughness for the T-peel test (because two peel arms are involved).

It can be seen that both external energy and plastic bending energy are strongly dependent on the peel angle, whilst adhesive fracture toughness has only a small reduction with increasing peel angle. This is commensurate with an increasing contribution from adhesive failure, together with some additional uncertainty associated with a larger plastic energy correction with increasing peel angle.

Figure 15 shows a similar style of presentation for the results for adhesive A. The variation in the plane of fracture for adhesive A is less pronounced; in all cases there is a combination of cohesive and adhesive failure. However, the 45°-fixed-arm peel results exhibit the highest amount of cohesive failure; this is probably commensurate with its higher value for adhesive fracture toughness. Again, the level of plastic energy correction is large throughout and, therefore, some uncertainty relates to all values of G_A.

Mandrel Peel

Mandrel peel tests were conducted on both adhesive systems. Illustrative results are shown in Figure 16 for adhesive F, following the scheme shown in Figure 5.

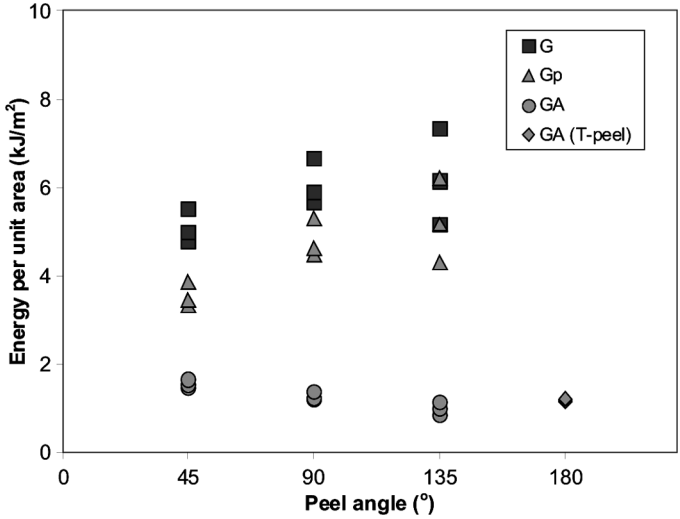

FIGURE 15 Results for adhesive A for the fixed-arm and T-peel tests.

Two tests are conducted; one with a bonded sample and another with an unbonded peel arm. The unbonded sample enables the slope of the peel force per unit width *versus* alignment force per unit width

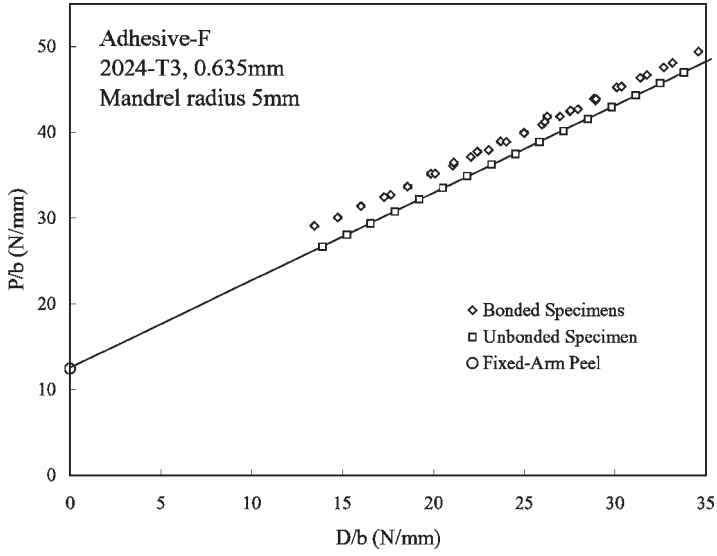

FIGURE 16 Illustrative Mandrel peel data for adhesive F.

plot to be defined (relating to the coefficient of friction in the instrument). Provided that the peel arm is fully conforming to the roller, then the slope of the peel force per unit width *versus* alignment force per unit width for the bonded sample will be the same, that is, the two plots are parallel. This then enables the plastic work in bending and the adhesive fracture toughness to be determined [9, 10]. The small displacement of force per unit width between the two curves is an indication of a high plastic bending energy. This is analogous to a large plastic correction discussed for the other peel tests.

It was necessary to use the smallest mandrel radius (5 mm) to ensure conformation to the mandrel roller. After the completion of data collection for a mandrel test on the bonded specimen, the mandrel was removed and a 90°-fixed-arm peel test was conducted. This result is plotted in Figure 16.

Alternative forms for presenting the mandrel results involved determining adhesive fracture toughness for each data point and then plotting G_A *versus* alignment force per unit width. Figures 17 and 18 show examples of these plots for both adhesive samples.

The planes of fracture were also observed for these laminates. For adhesive F, the peel failure was entirely cohesive at small alignment forces but gradually became more adhesive as the alignment force increased. This is completely reflected by the results in Figure 17. At small alignment forces, the adhesive fracture toughness is highest but gradually reduces as more adhesive failure is introduced in the peel process. Therefore, to obtain a cohesive value of adhesive fracture

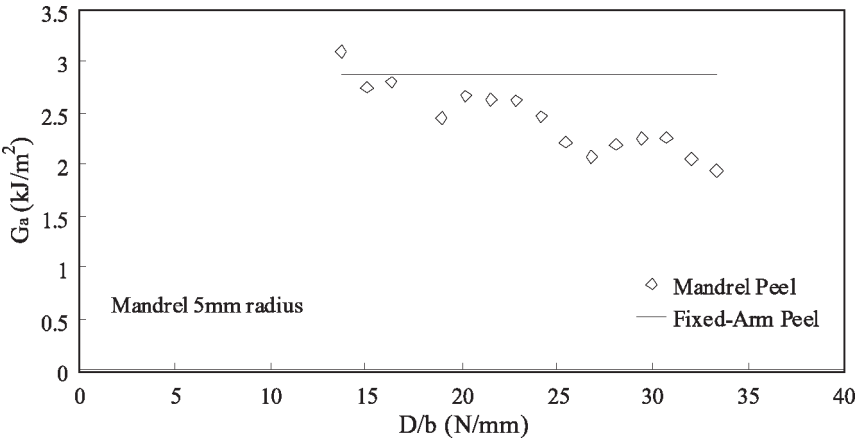

FIGURE 17 Adhesive fracture toughness for adhesive F from a mandrel peel test.

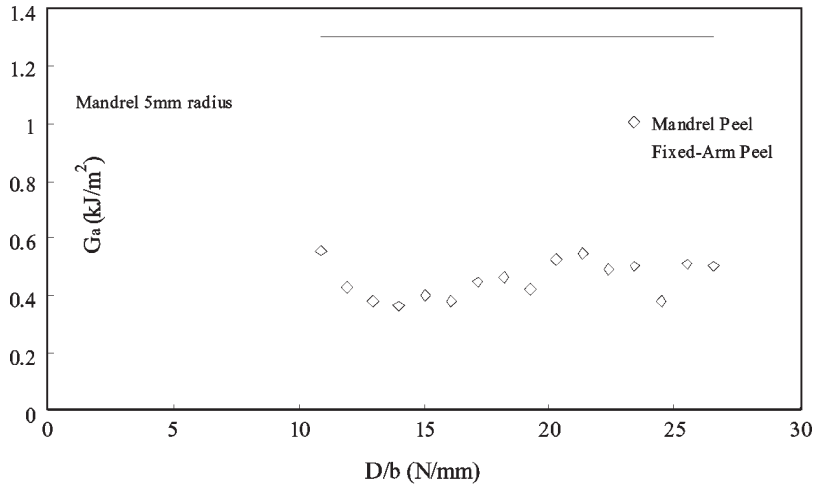

FIGURE 18 Adhesive fracture toughness for adhesive A from a mandrel peel test.

toughness for adhesive F, the curve in Figure 16 or 17 was extrapolated to zero alignment force. This was slightly easier for plots of G_A *versus* D/b than for plots of P/b *versus* D/b. For the latter, although the slope of the line could be defined from the unbonded specimen, the location of the line for the bonded specimen was more problematic. This inevitably introduces some uncertainty in the determination of the cohesive fracture toughness value.

The 90°-fixed-arm peel test conducted on the mandrel jig also exhibited a combination of adhesive and cohesive fracture (similar to that for the 90°-fixed-arm test conducted on the variable-angle fixed-arm peel apparatus). Hence, the zero alignment force adhesive fracture toughness from the mandrel test is higher than the 90°-fixed-arm peel test value, as shown in Figures 16 and 17.

Comparing the fixed-arm data (for a peel angle of 90°) in Figure 16 with the schematic in Figure 5 shows that the force per unit width (and hence G_A) at $D/b = 0$ is at variance. Theory (Figure 5) anticipates a higher value for F/b at $D/b = 0$ whilst observation from the fixed arm data has F/b smaller at $D/b = 0$ (Figure 16). The reason for this is entirely because of the change in the plane of fracture. In the 90°-fixed-arm test, the fracture was partially adhesive, whilst the anticipated zero alignment force fracture in the mandrel test would be cohesive. (A cohesive value for G_A will be higher than an adhesive value.)

The mandrel peel test conducted on the laminate specimen based on adhesive A showed considerable adhesive failure. Therefore, the G_A value shown in Figure 18 is quite small. However, the plane of fracture for the 90°-fixed-arm peel test showed a much higher level of cohesive fracture, although it was still a mixture of cohesive and adhesive failure. Therefore, the adhesive fracture toughness value from the fixed-arm peel test shown in Figure 18 is significantly higher than the value from the mandrel peel.

Further details of the planes of fracture are discussed in the next section.

Comparison of Results from Different Test Methods

Five different test methods have been used to measure the adhesive strength of the AA/toughened epoxy laminates. Each method involved a peel process and the aim has been to determine adhesive fracture toughness from each of the approaches. The climbing-drum method did not yield a valid value for adhesive fracture toughness because the peel arm did not conform to the roller and the nonconformance could not be measured. However, the other four methods did furnish values for adhesive fracture toughness and these values can now be compared for the two adhesives.

Before making a quantitative comparison, it should be recalled that the plane of fracture was different in these various methods. To rationalise these differences, a scale of failure has been devised whereby a fully cohesive fracture is designated a mark of 10 and a fully adhesive fracture is designated a mark of 1. Adopting this somewhat simplified index, it is possible to compare the various fracture modes for the two adhesive samples. Naturally, this is a subjective way of describing the nature of the plane of fracture. However, it is adequate for the purposes required here, particularly as an alternative and more objective approach is far from straightforward.

Figure 19 shows the fracture index (1–10) with optical micrographs of the peeled surfaces. It is apparent that the index used to describe the plane of failure is simplistic; however, the figure captures the range of planes of fracture observed in the tests. It can be expected that the values of adhesive fracture toughness will be influenced by the changes in fracture mode.

Figure 20 shows a similar set of optical micrographs for adhesive A where the index range is much narrower because all planes of fracture were totally or partially adhesive.

The narrower range of failure types for adhesive A should also be reflected in a closer grouping for the measured adhesive fracture toughness values.

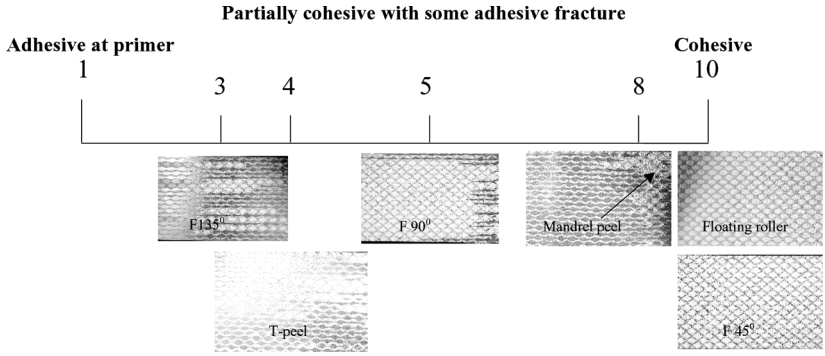

FIGURE 19 Planes of fracture for adhesive F for the various tests. (F45°, F90°, and F135° refer to specimens from the fixed-arm tests at these peel angles. For the mandrel test micrograph, the arrow indicates the start of the peel process because the plane of fracture changed as alignment force increased.)

It is now possible to compare the adhesive fracture toughness values (G_A) from each of the tests, whilst recognising that some failures are cohesive and some are adhesive. However, a complementary property for the adhesive fracture toughness value is the cohesive

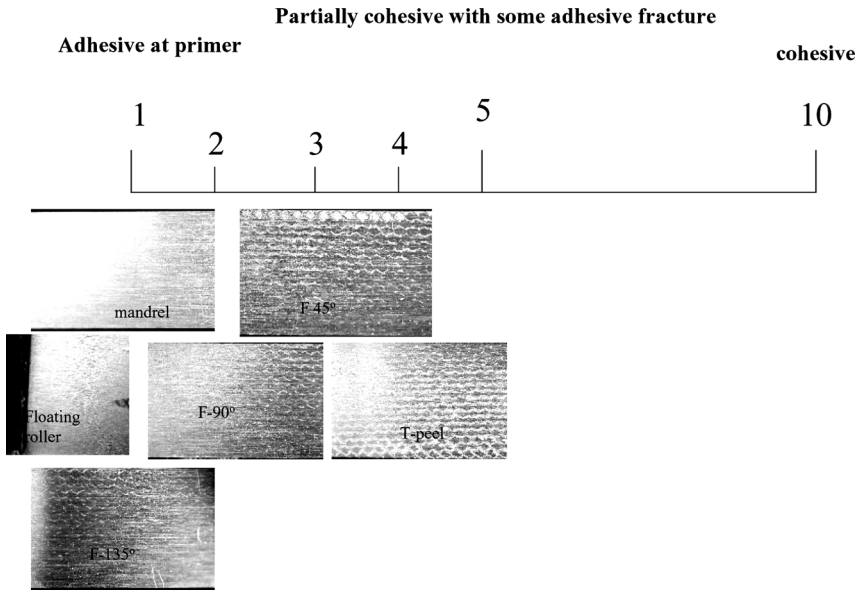

FIGURE 20 Planes of fracture for adhesive A for the various tests. (F45°, F90°, and F135° refer to specimens from the fixed-arm tests at these peel angles.)

fracture toughness for the adhesive (G_C). A procedure based on a tapered double cantilever beam (TDCB) mode I fracture test has been established for this [13] and values for G_C have been obtained to make comparison with the G_A values from the peel tests. Some of the peel cracks relate to an adhesive mechanism where the crack runs at or near to the substrate surface. In these circumstances, it could be argued that the plastic zone is only sufficient to create half of a fully developed inelastic zone at the crack tip. Therefore, for so-called adhesive fractures, it could be argued that the fracture toughness is half the cohesive value, at the most. Consequently, values of G_A associated with adhesive fractures that are greater than the half value of G_C imply that fracture is near the interface but not at the interface. In the two figures that follow, both cohesive and adhesive fracture toughness values are included for comparison with the adhesive fracture toughness values from the peel tests.

All of the toughness values for adhesive F are shown in Figure 21. Included with each set of data points is the fracture index from Figure 19. The cohesive toughness value from the TDCB test and

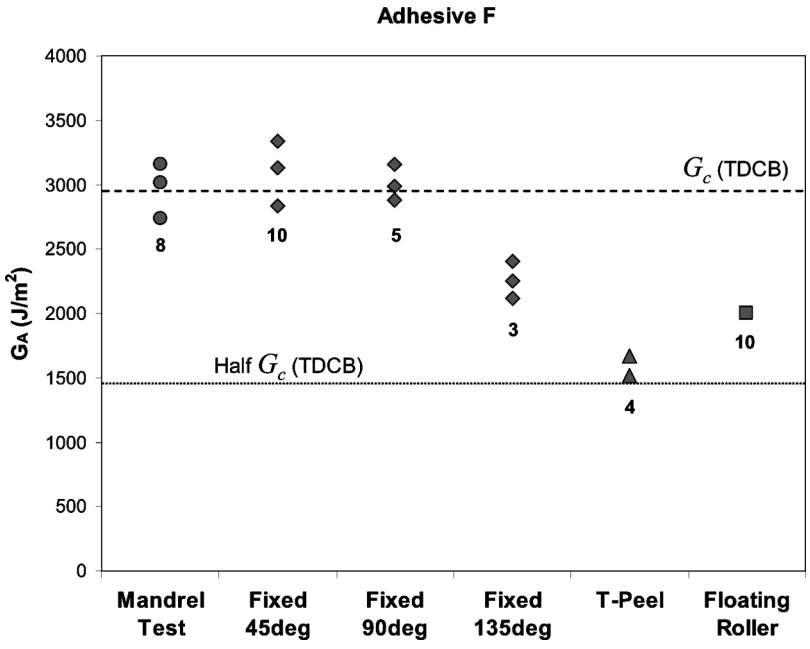

FIGURE 21 Adhesive fracture toughness and cohesive fracture toughness for adhesive F. (The numbers refer to the fracture index.)

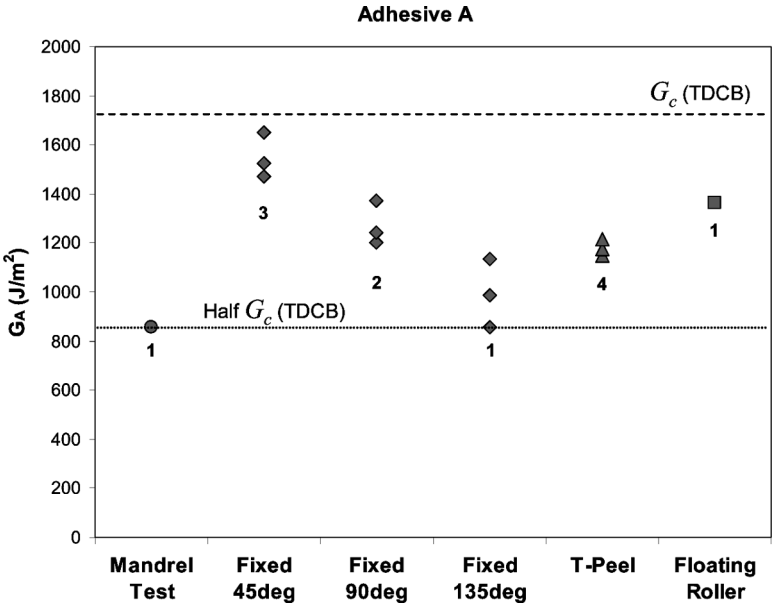

FIGURE 22 Adhesive fracture toughness and cohesive fracture toughness for adhesive A. (The numbers refer to the fracture index.)

half of this value are also shown. It is apparent that adhesive fracture toughness is not common for the four peel methods. However, the plane of fracture for the 135°-fixed-arm peel and the T-peel exhibit a significant contribution from adhesive failure. Therefore, it is not surprising to observe lower G_A values from these tests. These adhesive failures exhibit a peel fracture toughness that shows some agreement with fracture toughness for interfacial failures. The floating-roller test required measurement of the radius of curvature of the peel arm and it is possible that this introduced additional experimental error. Nevertheless, the cohesive failures in the mandrel and in the fixed-arm tests at peel angle of 45° and 90° show agreement with the measured cohesive fracture toughness from the TDCB test.

Figure 22 shows a similar presentation of results for adhesive A. On this occasion, all of the adhesive fracture toughness results exhibit various levels of adhesive failure. Consequently, all values of adhesive fracture toughness are, as expected, less than the cohesive fracture toughness value from a TDCB test. However, the most adhesive fractures (with fracture index 1) show good agreement with half the cohesive fracture toughness. The magnitude of

adhesive fracture toughness approximately reflects the degree of adhesive failure in the peel fracture surface. T-peel and 45°-fixed-arm peel specimens exhibit the highest contributions from cohesive failure. It is possible that the large plastic bending energy corrections accounts for the remaining scatter.

CONCLUDING COMMENTS

A principal aim of this work is to comment on the assessment of metal–epoxy laminates for aerospace applications. In this context, it is appropriate to include two regular assessment schemes in the form of the floating-roller and climbing-drum peel tests. It was observed that, in both of these methods, the peel arm did not conform to the roller. Therefore, both methods are invalid because the variability associated with nonconformance can only introduce scatter to the results. In addition, it is observed that the level of plastic bending energy associated with peel is of the order of 75% to 90%. Consequently, the use of just peel strength, which is related to the external work associated with peeling, is an inadequate description of the adhesive strength. Adhesive fracture toughness would be more appropriate, but the nonconformance of the peel arm in these standard tests frustrates such a calculation.

A unified theory has been developed that accommodates all of the five peel test methods and preliminary experimental observations support this theory. However, further and more detailed work is needed.

In the case of the floating-roller test, it is possible to observe the peel arm in an adjacent manner during the test. Therefore, measurement of the radius of curvature of the peel arm is possible and, in turn, a determination of the adhesive fracture toughness can be made. The theory accommodates the conditions for conformance of the peel arm to the roller and experimental observation supports these findings.

Both fixed-arm and T-peel test methods can be used to determine adhesive fracture toughness; that is, a correction for plastic bending energy can be made. Observations in these tests show variable planes of fracture and it is possible that the occurrence of adhesive failure might be an inherent feature in the assessment of these aerospace laminates. Moreover, it would seem that a comprehensive evaluation of aerospace laminates might need to include adhesive (type and thickness), primer (type and thickness), and substrate (type and thickness). In this manner, it might be possible to evaluate a rationale where adhesive and cohesive planes of fracture were assessed, and, in turn, to obtain a more credible evaluation of the laminate system.

Mandrel peel procedures have been successfully used for these laminate systems. Moreover, the mandrel test provides a direct experimental determination of adhesive fracture toughness and does not invoke complex analytical or numerical calculations. It is concluded that it offers potential for a new procedure of assessment for these laminates. However, further work is required on different geometric aspects (such as roller radius) and laminate variables (such as primer thickness and substrate thickness).

Overall, the agreement between adhesive fracture toughness from the various test methods is encouraging, even though the plastic corrections are large and despite a varying plane of fracture.

ACKNOWLEDGEMENTS

The authors acknowledge support from an EPSRC Platform grant, support for D. R. Moore from a Royal Academy of Engineering senior research fellowship, and support for L. F. Kawashita from IMRE, Singapore.

REFERENCES

[1] The American Society for Testing and Materials (ASTM) D 1781-93, *Standard Test Method for Climbing Drum Peel for Adhesives* (1993).
[2] The American Society for Testing and Materials ASTM D 3167-97, *Standard Test Method for Floating Roller Peel Resistance of Adhesives* (1997).
[3] Kinloch, A. J., Lau, C. C., and Williams, J. G., *Int. J. Fract.* **66**, 45–70 (1994).
[4] Lau, C. C., A fracture mechanics approach to the adhesion of packaging laminates, Ph.D. Thesis, University of London (1993).
[5] Georgiou, I., Hadavina, H., Ivankovic, A., Kinloch, A. J., Tropsa, V., and Williams, J. G., *J. Adhes.* **79**, 1–27 (2003).
[6] Moore, D. R. and Williams, J. G., in *Proc. ESIS 3rd Conference on Fracture of Polymers, Adhesives and Composites*, B. R. K. Blackman, A. Pavan, and J. G. Williams (Eds.), ESIS Pub 32, (Elsevier, Oxford, 2003).
[7] The American Society for Testing and Materials (ASTM) D 1876-95 9, *Standard Test Method for Peel Resistance of Adhesives (T-Peel).* (1995).
[8] The American Society for Testing and Materials (ASTM) D903-98, *Standard Test Method for Peel or Stripping Strength of Adhesive bonds* (1998).
[9] Kawashita, L. F., Moore, D. R., and Williams, J. G., *J. Adhes.* **80**, 1–21 (2004).
[10] Breslauer, E. and Trocynski, T., *J. Adhes. Sci. Technol.* **12**(4), 367–382 (1998).
[11] Moore, D. R. and Williams, J. G., in *Fracture Mechanics Testing Methods for Polymers, Adhesives and Composites,* D. R. Moore and J. G. Williams (Eds.) (Elsevier, Oxford, 2001), Chap. 3, p. 203.
[12] Blackman, B. and Kinloch, A. J., in *Fracture Mechanics Testing Methods for Polymers, Adhesives and Composites*, D. R. Moore, A. Pavan, and J. G. Williams (Eds.) (Elsevier, Oxford, 2001), Chap. 3, p. 225.